Cluster formation and phase transition in nuclear disassembly using a variety of clusterization algorithms

Samiksha Sood,[1] Rohit Kumar,[1,*] Arun Sharma,[2] and Rajeev K. Puri[1,†]
[1]*Department of Physics, Panjab University, Chandigarh 160014, India*
[2]*G.D. College, Thanna Mandi, Rajouri, Jammu and Kashmir-185212, India*

(Received 3 April 2018; revised manuscript received 2 March 2019; published 13 May 2019)

The reactions of $^{40}\mathrm{Ar} + {}^{45}\mathrm{Sc}$ are studied using the quantum molecular dynamics (QMD) model at various incident energies. The phase space generated using the QMD model is coupled with various clusterization algorithms to identify fragments. The obtained charge yield of intermediate mass fragments ($3 \leqslant Z_f \leqslant 12$) is fitted with power law [$Y(Z_f) \propto Z_f^{-\tau}$] and exponential fits [$Y(Z_f) \propto e^{-\lambda Z_f}$] in search of critical behavior. We also analyzed other critical parameters based on the moments and the charge of the second largest fragment. Our detailed study indicates that the extraction of the critical point of the liquid-gas phase transition is nearly insensitive towards different spatial-based clusterization algorithms, freeze-out time, as well as towards different binding energies at microlevels.

DOI: 10.1103/PhysRevC.99.054612

I. INTRODUCTION

The similarity between nucleon-nucleon interactions (short-range repulsive and long-range attractive parts) and the Van der Waal's forces between molecules indicates the existence of a liquid-gas phase transition in excited nuclear matter [1–18]. Conversely, based on the similarity between the equations of state for both phases (that differs approximately by five orders of magnitude), it is considered that, like liquid-gas phase transition in macroscopic systems, multifragmentation phenomenon must also contain some signals of the phase-transitions in nuclear matter [1–18]. In this direction, it was found that the mass/charge yields when fitted as a function of mass (A_f)/charge (Z_f) obey a power law [$\mathrm{Y}(A_f) \propto {A_f}^{-\tau}/\mathrm{Y}(Z_f) \propto {Z_f}^{-\tau}$] at a certain excitation energy; the plausible signal of the liquid-gas phase transition in nuclear matter [3–18]. Such a signal was first noted by the Pioneer Purdue group [9]. Later on, this behavior was also reported by various other theoretical groups and was found to be in accordance with the earlier predictions of the Fisher's droplet model [3,5–7,10,11]. It is worth mentioning that the occurrence of a phase transition in multifragmentation phenomenon was also questioned in some studies. The study conducted by Porile *et al.* [19] presented one such classical example.

The occurrence of the phase transition in nuclear matter has been predicted using two different approaches: (i) Using those models that predict the phase transition based on the breaking of nuclear matter at subnormal densities and (ii) using the evolution of the decay mechanism of nuclei as a function of excitation energy. Though the former one is purely a theoretical concept, the latter one, however, can be used to pin down the phase transition experimentally as well [3–12,17,18]. In the present work, we will focus on the latter method. In this method, the critical point of the phase transition (also termed as the onset of multifragmentation) corresponds to a minimum in the value of the critical parameter (τ) when plotted as a function of incident energy [9–12,14,18]. For example, Li *et al.* [10] reported experimental findings of the charge spectra of fragments emitted in the reactions of $^{40}\mathrm{Ar} + {}^{45}\mathrm{Sc}$ and observed a minimum in the critical exponent (τ) at incident energy of 23.9 ± 0.7 MeV/nucleon. The percolation model was also used in this study for theoretical understanding [10,11]. In another experiment, Ogilvie *et al.* [8] reported the existence of the above minimum in the Au induced reactions on C, Al, and Cu targets at incident energy of 600 MeV/nucleon. Similarly, William *et al.* [2] performed the experiment for the reaction of $^{84}\mathrm{Kr} + {}^{197}\mathrm{Au}$ and compared their results to the statistical multifragmentation model (SMM). It is worth mentioning that some studies use exponential fits [$Y(Z_f) \propto e^{-\lambda Z_f}$] rather than power-law fits [$Y(Z_f) \propto Z_f^{-\tau}$] to extract the corresponding minimum [1,8,10,11].

Among various transport models, n-body theories such as the quantum molecular dynamics (QMD) model [20] and its isospin-dependent variant [21] enjoy special status since they can preserve the individual correlations among the nucleons. These models were also used couple of times in the past to get glimpse of the phase transition [3,5,22,23]. In one of such studies, Ma *et al.* [3] used the QMD model and reported a minimum in τ at 65 MeV/nucleon for the reactions of $^{40}\mathrm{Ar} + {}^{27}\mathrm{Al}$. On the other hand, Puri *et al.* found a flat behavior of the power-law parameter τ for the reaction of $^{40}\mathrm{Ar} + {}^{45}\mathrm{Sc}$ using the isospin-dependent quantum molecular dynamics (IQMD) model [22].

In some studies, it was pointed out that the power-law observation of the mass (charge) distribution is necessary, but not a sufficient condition for extracting the phase transition or

*rohitksharma.pu@gmail.com
†rkpuri@pu.ac.in

critical point in a heavy-ion reaction. Therefore, various other quantities such as the moments of the charge distribution, the Campi scatter plots, the multiplicity derivative of the fragment multiplicity, as well as the fluctuation in the charge of the largest fragment and the second largest fragment and so on have also been put forward [4–7,14–16]. Belkacem *et al.* performed a detailed study of these parameters for the reaction of ^{197}Au + ^{197}Au at 35 MeV/nucleon using the classical molecular dynamics (CMD) model [7]. In another study, Ma *et al.* [4,5] examined the reactions of ^{40}Ar on ^{27}Al, ^{48}Ti, ^{58}Ni at 47 MeV/nucleon using the TAMU neutron ion multidetector for reaction oriented dynamics (NIMROD) setup for various critical parameters [4,5].

Interestingly, only a few studies discussed the influence of input parameters as well as fragment formation criteria on the critical exponent. For example, Li *et al.* [11] varied the initial lattice size from 50 to 800 in percolation model calculations and found a shift in the minimum of τ till lattice size of 500 and no effect was recorded afterwards. In another study, Pan *et al.* [12] varied the critical density (at which fragments are assumed to be formed) in the percolation model and reported a similar effect. In a recent study, Lin *et al.* examined the sensitivity of various phase transition parameters for primary and secondary fragments using statistical multifragmentation model (SMM) calculations [14]. They showed that the analysis of primary and secondary fragments can influence the critical point observation. The importance of the simultaneous study of various critical parameters was also put forward.

It should be noted that all the above-mentioned dynamical studies were conducted by employing the minimum spanning tree (MST) method as a fragment identifier [3–5,7,22–24]. At the same time, improvements over the MST method were also reported time to time [3,4,20,25–31]. These modifications range from the simple momentum cut to complicated energy minimization. We must also keep in mind that the clusterization method is enforced at a certain reaction time to identify fragments. Therefore, one has to also examine the phase transition by keeping in mind the associated questions such as freeze-out time, initialization, parameters of the clusterization algorithm, and so on. In this work, we will focus on the role of these improvements (over the MST method) in deciding the phase transition in heavy-ion reactions.

This paper is organized as follows. In Sec. II, we present brief details of the n-body dynamical model along with various clusterization techniques to be used in the present work. The results are discussed in Sec. III followed by a summary in Sec. IV.

II. MODEL

The QMD model [20] is a microscopic n-body dynamical model used to simulate a heavy-ion collision on an event-by-event basis. In this model, each nucleon, represented by a Gaussian wave packet, propagates using the Hamilton's classical equations of motion

$$\dot{\mathbf{r}}_i = \nabla_{\mathbf{p}_i} H; \quad \dot{\mathbf{p}}_i = -\nabla_{\mathbf{r}_i} H. \tag{1}$$

Here Hamiltonian H consists of the kinetic and potential terms. The potential term mimic the two- and three-body interactions in terms of density functionals. In this study, a soft equation of state together with energy-dependent cross-section is used [20,25,26,28–32]. The information about the phase space generated by the QMD model is then injected into various clusterization algorithms discussed in the following paragraphs.

A. Minimum spanning tree method

The MST method [20] identifies various fragments on the basis of the distance among its constituent nucleons. Accordingly, two nucleons share the same fragment if their distance is less than 4 fm, i.e.,

$$|\mathbf{r}_i - \mathbf{r}_j| \leqslant 4\,\text{fm}, \tag{2}$$

where $\mathbf{r}_i$ and $\mathbf{r}_j$ are the centroids of the nucleons in coordinate space.

B. Minimum spanning tree method with momentum cut

To avoid the formation of loosely bound/unbound fragments, the relative momenta of the nucleons is also constrained in addition to their coordinate space [28,29]. Accordingly, we demand

$$|\mathbf{r}_i - \mathbf{r}_j| \leqslant 4\,\text{fm}; \;\; |\mathbf{p}_i - \mathbf{p}_j| \leqslant \mathbf{p}_{\text{Fermi}}, \tag{3}$$

where $\mathbf{p}_i$ and $\mathbf{p}_f$ are the momentum coordinates of the ith and jth nucleons and $\mathbf{p}_{\text{Fermi}}$ is the Fermi momentum.

C. Binding-energy-based clusterization algorithm

In this algorithm a more realistic approach is considered where the realization of the fragment structure depends on the interactions and relative kinetic energy of the nucleons of a fragment identified by the MST method. The following mechanism is adopted for identifying such realistic fragments.

(1) Identify the clusters using the MST method and
(2) Then subject each such fragment to the following binding energy check:

$$\zeta = \sum_{i=1}^{A_f} \left[\frac{\left(\mathbf{p}_i - \mathbf{p}_{A_f}^{\text{c.m.}}\right)^2}{2m} + \frac{1}{2}\sum_{j\neq i}^{A_f} V_{ij}(\mathbf{r}_i, \mathbf{r}_j) \right] < E_{\text{bind}}. \tag{4}$$

In the above equation, A_f and $\mathbf{p}_{A_f}^{\text{c.m.}}$ represent the total number of nucleons in a cluster and center-of-mass momentum of that cluster, respectively. The probability of the fragment sustainability depends on the E_{bind} (binding energy) [26,27,30,31]. Generally, one can use the binding energy corresponding to a cold or hot nucleus. Two of us have already shown that one should implement thermal binding energies instead of cold binding energies to filter the unstable fragments (for details see Refs. [30,31]) at the time of their identification. We will continue with this approach in this work also and will implement only temperature-dependent binding energies to filter the unstable fragment structures. Interestingly, for the hot binding energies, various formulas were proposed in the literature [33–35]. We shall discuss some of these formulas in the following paragraphs [26,30].

TABLE I. Parameters of the temperature-dependent binding energy formulas of Pi *et al.* [34] and Sauer *et al.* [35] used in the present work. All values are in MeV.

Label	a_v	a_s	a_c	$a_{\rm sym}$	α_v	α_s	$\alpha_{\rm Coul}$	$\alpha_{\rm sym}$	a_{ss}	α_{ss}
Pi *et al.*	16.00	20.80	0.7714	33.960	0.064	0.2238	0.00102	71.50	71.54	0.8184
Sauer *et al.*	16.10	19.00	0.7000	30.020	0.055	0.1500	0.00070	60.04	0.0	0.0

In this method, the excitation energies of various fragments are taken into account and $E_{\rm bind}$ is calculated using the so-called temperature-dependent binding energy formulas. This method is dubbed as minimum spanning tree with thermal binding energy cut (MSTBT) [30,31]. Here we use three different temperature-dependent binding energy formulas proposed by Davidson *et al.* [33], Pi *et al.* [34], and Sauer *et al.* [35]. A few details of the temperature-dependent binding energy formulas are as followings.

The first formula put forward by Davidson *et al.* used the canonical ensemble theory. This formula reads as

$$\begin{aligned} E_{\rm Bind}(T) &= \alpha(T)A_f + \beta(T)A_f^{2/3} \\ &+ \left(\gamma(T) - \frac{\eta(T)}{A_f^{1/3}}\right)\frac{(4t_\varsigma^2 + 4|t_\varsigma|)}{A_f} \\ &+ 0.8076\frac{{Z_f}^2 R(0)}{A_f^{1/3}R(T)} \\ &\times \left(1 - \frac{0.7636}{Z_f^{2/3}} - 2.29\frac{R(0)^2}{\left[R(T)A_f^{1/3}\right]^2}\right) \\ &+ \delta(T)\frac{f(A_f, Z_f)}{A_f^{3/4}}, \end{aligned} \tag{5}$$

where $t_\varsigma = (2Z_f - A_f)/2$ represents the isospin asymmetry of a nucleus. To derive this formula, the excitation energy of a nucleus is fitted according to canonical ensemble theory and is converted into the temperature of the considered system.

The other formula implemented for filtering the loosely bound fragments is given as

$$\begin{aligned} E_{\rm Bind}(T) &= (a_v - \alpha_v T^2)A_f - (a_s - \alpha_s T^2)A_f^{2/3} \\ &- \left[a_c\left(1 - \frac{a_{\rm Coul}}{A_f^{2/3}}\right) - \alpha_{\rm Coul}T^2\right]\frac{Z_f^2}{A_f^{1/3}} \\ &- (a_{\rm sym} - \alpha_{\rm sym} \times 10^{-4}T^2)\frac{(A_f - 2Z_f)^2}{A_f} \\ &+ (a_{ss} + \alpha_{ss}T^2)\frac{(A_f - 2Z_f)^2}{A_f^{4/3}}. \end{aligned} \tag{6}$$

This formula was proposed by Sauer *et al.* [35] and Pi *et al.* [34] using two different theories. Sauer *et al.* obtained this formula by employing the thermal Hartree-Fock approximation (TDHF), whereas Pi *et al.* used hot Thomas-Fermi calculations. In the first case, the density of the nucleus was considered to be somewhat greater at the interior compared to its surface, but in the latter case, the density was considered to vary continuously from the interior to the surface. Also, Pi *et al.* considered the contribution of the surface nucleons towards the nuclear symmetry energy; in contrast to Sauer *et al.* who ignored this contribution. In the case of the formula by Sauer *et al.*, the coefficient $a_{\rm Coul}$ was set to be zero, whereas $a_{\rm Coul}$ was taken to be 3.1445 by Pi *et al.* We find that the formula proposed by Pi *et al.* is more accurate compared to Sauer *et al.* for lighter mass nuclei. The parameter set used in the formulas of Sauer *et al.* and Pi *et al.* are listed in Table I. On the contrary, the parameter set used in the binding energy formulas of Davidson *et al.* is extracted from the graphical representation reported in Ref. [33]. The versions of the MSTBT method with binding energy formulas of Davidson *et al.*, Pi *et al.*, and Sauer *et al.* are termed as MSTBT (3.1), MSTBT (3.2), and MSTBT (3.3), respectively. As far as the extraction of the temperature from nonequilibrated system (like typical heavy-ion collisions) is concerned, there are many methods listed in the literature that account for diffusion of the surface and so on [36]. However, the present formulas are valid upto 4 MeV only. Therefore, using thermal binding energies with fixed temperature is just a case study to understand whether one needs to look at excited fragments in a different way or not. Such assumptions were introduced in our previous work successfully [30].

III. RESULTS AND DISCUSSIONS

A. Influence of different clusterization algorithms on various critical parameters

It is well known that the identification of the fragments based on the spatial correlations should be done when the system is diluted and fragments are well separated. Therefore, in the present study, clusterization algorithms are enforced at a freeze-out time of 300 fm/c where fragments are well separated from each other.

In Fig. 1, we display the fragment charge spectra obtained in the central reactions of ^{40}Ar + ^{45}Sc at different incident energies between 15 and 115 MeV/nucleon. The results obtained using MST, MSTP, and MSTBT methods are represented by squares, circles, and inverted triangles, respectively. It should be noted that for the discussion of Figs. 1 to 3, MSTBT results correspond to the results of MSTBT (3.1) (at 4 MeV) version. From the figure, the well-known trends can be noted. The heavier fragments dominate the spectra at lower incident energies, which is taken over by the lighter fragments at higher incident energies. At the same time, one sees nearly no effect of different clusterization algorithms on the spectra [2,3,10,11].

Now to see how different algorithms can affect the critical point, the charge yield distribution of intermediate mass fragments is fitted with a power law ($\propto Z_f^{-\tau}$) and exponential fitting ($\propto e^{-\lambda Z_f}$) (not shown in Fig. 1 to maintain the clarity

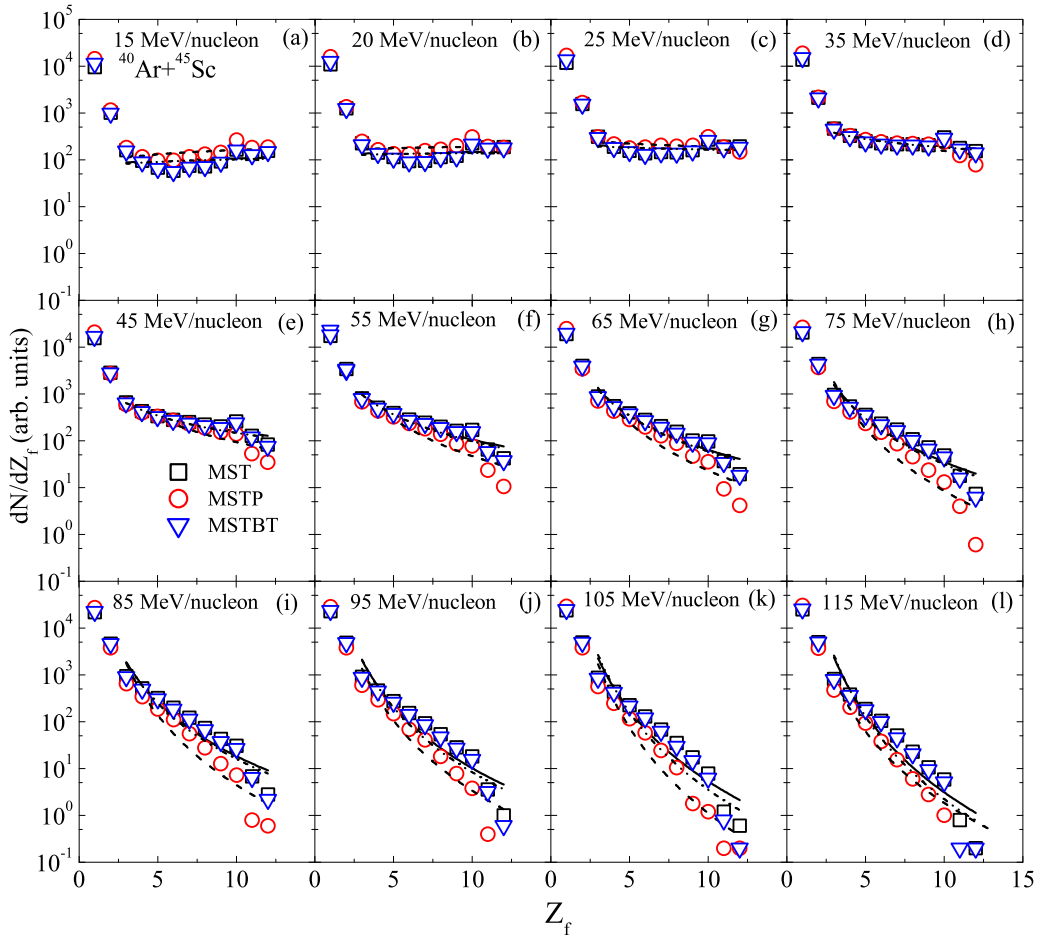

FIG. 1. The charge distributions of central reactions of $^{40}\mathrm{Ar} + {}^{45}\mathrm{Sc}$ at different projectile incident energies in the range of 15 to 115 MeV/nucleon. The open squares, open circles, and open, inverted triangles represent the results using the MST, MSTP, and MSTBT methods, respectively. The lines are to guide the eyes and correspond to power-law fits over fragment charge distributions for IMFs $[3 \leqslant Z_f \leqslant 12]$.

of the figure). In Fig. 2, the values of τ (upper panel) and λ (lower panel) obtained using different algorithms are plotted as a function of incident energy. Various symbols have the same meaning as in Fig. 1. In addition, the calculation with temperature of 2 MeV is also displayed in the figure (labelled as MSTBT′).

Looking at the Fig. 2, one notices that the value of $\tau(\lambda)$ increases with projectile's incident energy beyond 20 (25) MeV/nucleon; mimicking the increase in the sharpness of the charge spectra of the fragments. It is worth noting that even though the fragment charge yields (presented in Fig. 1) differ significantly for different algorithms, their power-law parameter τ (λ) shows almost similar trends with incident energy within error bars except for the MSTP method, where deviation is more significant. This happens due to a sharp decrease in the probability of the larger charge fragments. The minima in the $\tau(\lambda)$ is obtained using fourth-order polynomial fit as was done in Refs. [10,11,22,23]. The minima in τ (or critical point) is found at incident energies of 18.03, 19.04, and 18.03 MeV/nucleon using MST, MSTP, and MSTBT methods, respectively. Whereas no minima in τ is obtained in the case of MSTBT′ (inverted lined triangles) method. Similarly, for the exponential fits, the parameter λ has minima at incident energy of 21.06, 19.04, 19.04, and 17.02 using MST, MSTP, MSTBT, and MSTBT′ methods, respectively. It is worth mentioning that the values of τ (λ) are much lower than the experimentally measured or expected values. This may be due to the lack of exact Fermionic properties (such as specific heat) of the nucleons in the present dynamical model (see Refs. [37,38]). As mentioned above, the cold binding energies can also be enforced to check the stability of the fragments (dubbed as MSTB method) [26]. Though we already discarded its use in Ref. [30] here results with MSTB are also displayed for the reference purpose only. Interestingly, no minimum was observed when cold binding energies were used. This further shows that demanding cold binding energies for the fragment filtration is too stringent a condition. Probably one needs to wait longer to have cold fragments, but in that case, one runs into the risk of having spurious fragments. On the other hand, the use of thermal binding energy seems to be a reasonable condition. As noted, all different cluster identifiers reach nearly the same conclusion. It clearly demonstrates that the effect of different cluster identifiers is nearly insignificant.

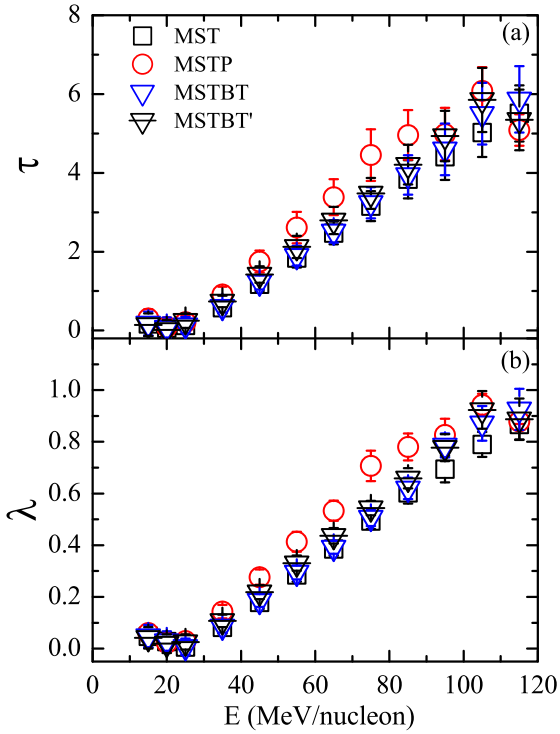

FIG. 2. The extracted values of power-law parameter τ (using power law fits [$Y(Z_f) \propto Z_f^{-\tau}$] and parameter λ (using exponential fits [$Y(Z_f) \propto e^{-\lambda Z_f}$] of IMFs as shown in Fig. 1) plotted as a function of incident energy. Different symbols carry the same meaning as in Fig. 1.

In a recent study, Lin *et al.* pointed that one should study various order parameters simultaneously to pin down the exact critical point [14]. Also the earlier studies showed that the occurrence of a minimum in $\tau(\lambda)$ is necessary but not a sufficient condition for the observation of phase transition [6]. Campi suggested using the moments of the charge distribution to pin down the critical point [15]. In general, the ith moment of the charge distribution having multiplicity "n" can be defined as

$$M_i = \sum_{Z_f \neq Z_{\max}} Z_f^i \; n(Z_f). \tag{7}$$

Here, Z_f is the charge and $n(Z_f)$ is the multiplicity of the fragment with charge Z_f in an event. The values obtained are then averaged over all events. In most of the studies two particular combinations of these moments are used namely normalized second moment (S_2) and γ_2 [4–7,13]. These are defined as

$$S_2 = \frac{M_2}{M_1}, \tag{8}$$

and

$$\gamma_2 = \frac{M_2 M_0}{M_1^2}, \tag{9}$$

where M_0, M_1, M_2 are the zeroth, first, and second moments of the charge distribution, respectively. In such an analysis, the parameters $\langle S_2 \rangle$ and $\langle \gamma_2 \rangle$ are expected to give maximal values at the critical point mimicking the largest fluctuations of the fragment charge distribution. Also due to the exclusion of largest cluster charge, one expects $\langle S_2 \rangle$ to be proportional to the isothermal compressibility [13]. In other studies, the charge of the second largest fragment ($\langle Z_{\max 2} \rangle$) is also found to show a maximal value at the critical point when plotted as a function of the incident energy of the projectile [5]. We also analyzed these parameters using various clusterization algorithms.

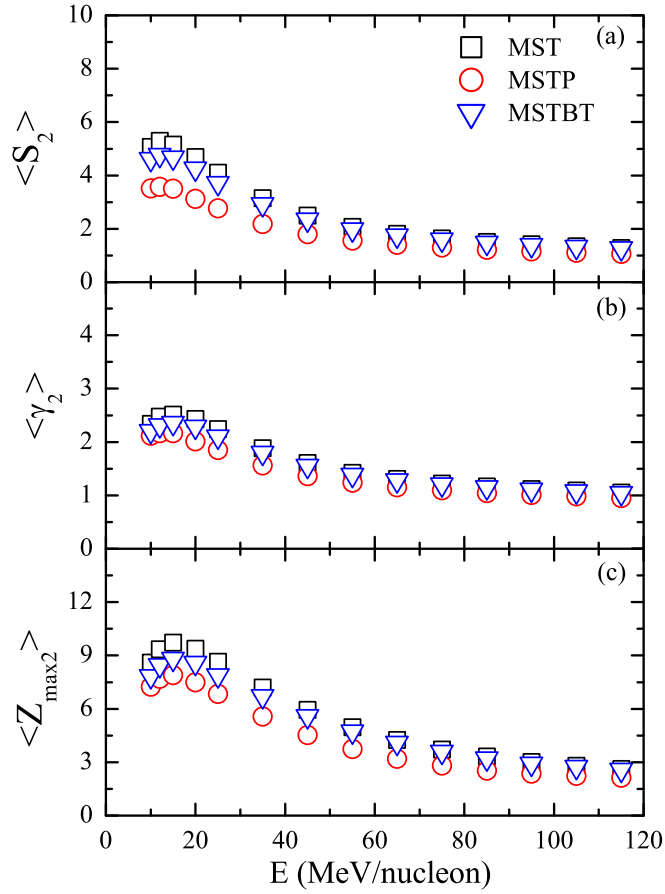

FIG. 3. The critical parameters $\langle S_2 \rangle$, $\langle \gamma_2 \rangle$ and $\langle Z_{\max 2} \rangle$ plotted as a function of the projectile incident energy using various clusterization algorithms. Symbols carry same meaning as in Fig. 2.

In Fig. 3, we display the values of the parameters $\langle S_2 \rangle$, $\langle \gamma_2 \rangle$, and $\langle Z_{\max 2} \rangle$ as a function of incident energy using MST, MSTP, and MSTBT methods. The symbols have the same meaning as in Fig. 2. We see that all three parameters give almost the same results over the entire range of the incident energy. The effect of different clusterization algorithms is nearly insignificant.

The parameter $\langle S_2 \rangle$ shows a maximal value at 12 MeV/nucleon for the fragments identified using MST, MSTP, and MSTBT methods. Note that this predicted critical point is much lower than the expected or measured value due to the inclusion of classical heat capacity in spite of the Fermionic one [38]. As pointed out in Ref. [38], the classical heat capacity is much larger than the Fermionic heat capacity, therefore, causing lesser production of IMFs and a larger

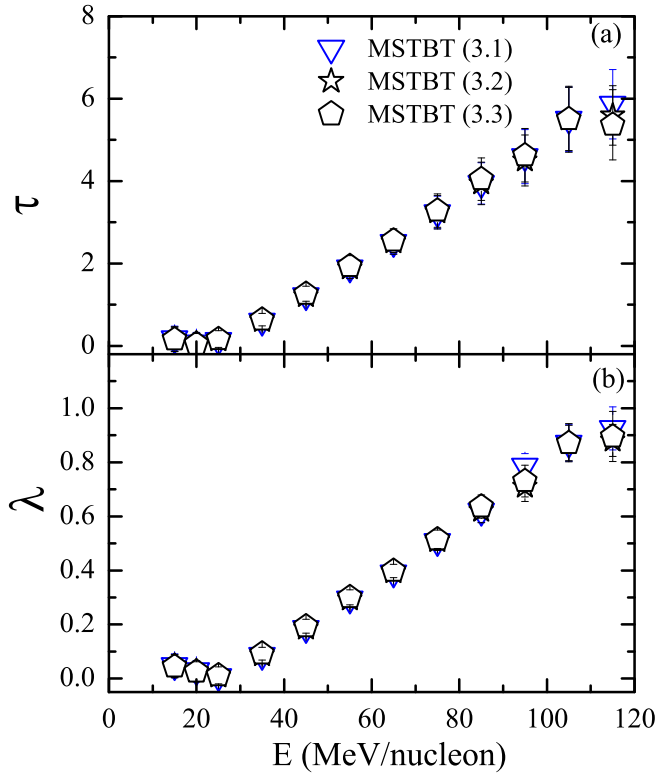

FIG. 4. Same as Fig. 2, but for the different thermal binding energy formulas implemented in the clusterization algorithm. Symbols are explained in the text.

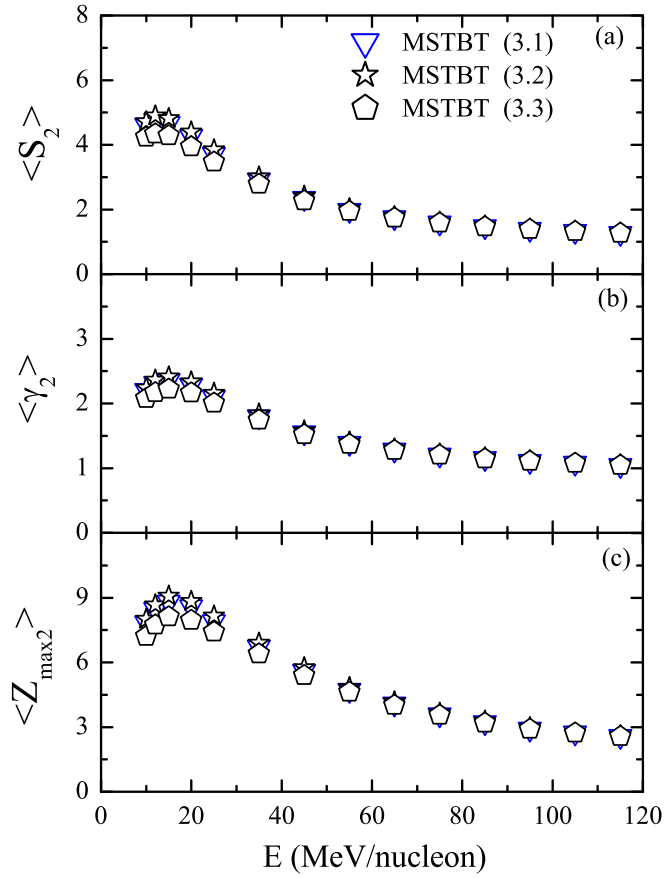

FIG. 5. Same as Fig. 3, but using different thermal binding energy formulas implemented in the clusterization algorithm.

Z_{max}. We also noted that the MST method gives highest value of $\langle S_2 \rangle$ due to maximum number of bound charge fragments.

Similarly, the parameters $\langle \gamma_2 \rangle$ and $\langle Z_{max2} \rangle$ show maxima at 15 MeV/nucleon using MST, MSTP, and MSTBT algorithms. It is worth mentioning that we also checked the sensitivity of our results by varying the freeze-out time from 300 to 400 fm/c. The critical values of $\tau(\lambda)$ read as 19.04 (20.05), 17.01 (18.03), and 21.06 (22.07) for MST, MSTP, and MSTBT methods, respectively. In other words, the effect of different freezing time is about 5−10% only. The effect is of similar order as we obtain for different clusterization algorithms.

On the other hand, no effect of different freeze-out time is seen on the other transition parameters such as $\langle S_2 \rangle$, $\langle \gamma_2 \rangle$, and $\langle Z_{max2} \rangle$. All these parameters remain completely insensitive towards both different clusterization algorithms as well as towards different freeze-out time (from 300 to 400 fm/c).

B. Effect of different thermal binding energies in clusterization algorithm

Now we would like to draw the attention of the reader to the studies conducted by Souza *et al.* [39] using the SMM and Karthikraj *et al.* [40] using the dynamical cluster model (DCM). In both these studies, results were reported depending on the binding energy formulas one uses in the analysis codes. Souza *et al.* conducted their study using the SMM model to constraint the symmetry energy using an isoscaling parameter based on the lighter fragments [39]. They took three liquid-drop-based binding energies, i.e., LDM1 [41], LDM2 [42], and LDM3 [43] to draw the breakup conditions for nuclei. The isoscaling parameter and thus, the symmetry energy was found to vary significantly with the choice of the binding energy formula in their analysis program. A similar type of results were reported by Karthikraj *et al.* but using different temperature-dependent binding energies in the DCM model to look for the α-structure of nuclei [40]. They studied the decay of the ^{56}Ni* compound nucleus formed in the reaction of $^{35}S + ^{24}Mg$. The α-structure was found to depend significantly on the temperature-dependent binding energy one is using in analysis code.

Keeping the above studies in mind, we extended our work by using different thermal binding energy formulas (discussed in Sec. II). We used MSTBT (3.1), MSTBT (3.2), and MSTBT (3.3) methods for analyzing the stable fragment structures and finally critical parameters namely, τ, λ, $\langle S_2 \rangle$, $\langle \gamma_2 \rangle$, and $\langle Z_{max2} \rangle$.

The results of τ and λ using different versions of MSTBT methods are plotted in Fig. 4, whereas Fig. 5 depicts the results for $\langle S_2 \rangle$, $\langle \gamma_2 \rangle$, and $\langle Z_{max2} \rangle$ parameters. The inverted triangles, stars, and pentagons represent the results obtained using MSTBT (3.1), MSTBT (3.2), and MSTBT (3.3) methods, respectively. From Fig. 4, we observe minima in τ at 18.03, 17.02, and 17.72 MeV/nucleon for MSTBT (3.1), MSTBT (3.2), and MSTBT(3.3) methods, respectively. For λ,

minima are obtained at 19.04, 20.05, and 19.04 MeV/nucleon for MSTBT (3.1), MSTBT (3.2), and MSTBT (3.3) methods, respectively.

All other parameters $\langle S_2 \rangle$, $\langle \gamma_2 \rangle$, and $\langle Z_{max2} \rangle$ (see in Fig. 5) show the insignificant effect of different versions of the MSTBT method. Our these results are in agreement with previously reported results [30,31].

IV. SUMMARY

In the present study, we investigate the connection between liquid-gas phase transition (or the onset of multifragmentation) and fragment charge yields for the central reactions of $^{40}\mathrm{Ar} + {}^{45}\mathrm{Sc}$. The present study is carried out using the quantum molecular dynamics model as phase-space generator coupled with different clusterization algorithms. Our detailed study clearly indicates that different quantities advocated to study the phase transition [namely the minimum in the critical parameter $\tau(\lambda)$ and maxima in $\langle S_2 \rangle$, $\langle \gamma_2 \rangle$ and $\langle Z_{max2} \rangle$] give nearly consistent results. Further, all these results are nearly insensitive towards different cluster algorithms, different freeze-out time, as well as towards different thermal binding energies formulas, and therefore, present a universal behavior.

ACKNOWLEDGMENT

This work is funded by the Council of Scientific and Industrial Research (CSIR), Government of India, via Grant No. 03 (1388)/16/EMR-II.

[1] G. Peilert, H. Stocker, W. Greiner, A. Rosenhauer, A. Bohnet, and J. Aichelin, Phys. Rev. C **39**, 1402 (1989).
[2] C. Williams *et al.*, Phys. Rev. C **55**, R2132 (1997).
[3] Y. G. Ma and W. Q. Shen, Phys. Rev. C **51**, 710 (1995).
[4] Y. G. Ma *et al.*, Phys. Rev. C **69**, 031604(R) (2004).
[5] Y. G. Ma, J. Phys. G: Nucl. Part. Phys. **27**, 2455 (2001).
[6] Y. G. Ma *et al.*, Phys. Rev. C **71**, 054606 (2005).
[7] M. Belkacem *et al.*, Phys. Rev. C **54**, 2435 (1996).
[8] C. A. Ogilvie *et al.*, Phys. Rev. Lett. **67**, 1214 (1991).
[9] J. E. Finn *et al.*, Phys. Rev. Lett. **49**, 1321 (1982).
[10] T. Li *et al.*, Phys. Rev. Lett. **70**, 1924 (1993).
[11] T. Li *et al.*, Phys. Rev. C **49**, 1630 (1994).
[12] J. Pan and S. D. Gupta, Phys. Rev. C **51**, 1384 (1995).
[13] J. Pan, S. Das Gupta, and M. Grant, Phys. Rev. Lett. **80**, 1182 (1998).
[14] W. Lin, P. Ren, H. Zheng, X. Liu, M. Huang, R. Wada, and G. Qu, Phys. Rev. C **97**, 054615 (2018).
[15] X. Campi, J. Phys. A **19**, L917 (1986).
[16] S. Mallik, G. Chaudhuri, P. Das, and S. Das Gupta, Phys. Rev. C **95**, 061601(R) (2017).
[17] M. D'Agostino *et al.*, Phys. Rev. Lett. **75**, 4373 (1995).
[18] M. Jandel, S. Wuenschel, D. V. Shetty, G. A. Souliotis, A. L. Keksis, S. J. Yennello, and M. Veselsky, Phys. Rev. C **74**, 054608 (2006).
[19] N. T. Porile *et al.*, Phys. Rev. C **39**, 1914 (1989).
[20] J. Aichelin, Phys. Rep. **202**, 233 (1991).
[21] C. Hartnack *et al.*, Eur. Phys. J. A **1**, 151 (1998).
[22] A. Sharma, A. Bharti, S. Gautam, and R. K. Puri, Nucl. Phys. A **945**, 95 (2016).
[23] A. Sharma and A. Bharti, Eur. Phys. J. A **52**, 42 (2016).
[24] R. Kumar, S. Sood, A. Sharma, and R. K. Puri, Acta Phys. Pol. B **49**, 301 (2018).
[25] R. K. Puri, C. Hartnack, and J. Aichelin, Phys. Rev. C **54**, R28 (1996); R. K. Puri and J. Aichelin, J. Comput. Phys. **162**, 245 (2000); R. Kumar and R. K. Puri, Phys. Rev. C **97**, 034624 (2018).
[26] S. Kumar and R. K. Puri, Phys. Rev. C **58**, 2858 (1998); S. Goyal and R. K. Puri, *ibid.* **83**, 047601 (2011).
[27] R. Kumar *et al.*, Eur. Phys. J. A **52**, 112 (2016).
[28] S. Kumar and R. K. Puri, Phys. Rev. C **58**, 320 (1998).
[29] J. Singh, S. Kumar, and R. K. Puri, Phys. Rev. C **63**, 054603 (2001).
[30] R. Kumar, S. Gautam, and R. K. Puri, Phys. Rev. C **89**, 064608 (2014).
[31] R. Kumar, S. Gautam, and R. K. Puri, J. Phys. G: Nucl. Part. Phys. **43**, 025104 (2016).
[32] Y. K. Vermani and R. K. Puri, Europhys. Lett. **85**, 62001 (2009); C. Dorso and J. Randrup, Phys. Lett. B **301**, 328 (1993); Y. K. Vermani *et al.*, J. Phys. G: Nucl. Part. Phys. **37**, 015105 (2010).
[33] N. J. Davidson *et al.*, Phys. Lett. B **315**, 12 (1993); N. J. Davidson, Nucl. Phys. A **570**, 61 (1994).
[34] M. Pi, X. Vinnas, and M. Barranco, Phys. Rev. C **26**, 733 (1982).
[35] G. Sauer, H. Chandra, and U. Mosel, Nucl. Phys. A **264**, 221 (1976).
[36] R. K. Puri *et al.*, Nucl. Phys. A **575**, 733 (1994).
[37] H. Feldmeier and J. Schnack, Rev. Mod. Phys. **72**, 655 (2004).
[38] R. Donangelo, H. Schulz, K. Sneppen, and S. R. Souza, Phys. Rev. C **50**, R563 (1994).
[39] S. R. Souza, M. B. Tsang, R. Donangelo, W. G. Lynch, and A. W. Steiner, Phys. Rev. C **78**, 014605 (2008).
[40] C. Karthikraj, N. S. Rajeswari, and M. Balasubramaniam, Phys. Rev. C **86**, 014613 (2012).
[41] M. A. Preston and R. K. Bhaduri, *Structure of the Nucleus* (Addison-Wesley, Reading, MA, 1975).
[42] S. R. Souza, P. Danielewicz, S. DasGupta, R. Donangelo, W. A. Friedman, W. G. Lynch, W. P. Tan, and M. B. Tsang, Phys. Rev. C **67**, 051602(R) (2003).
[43] P. Danielewicz, Nucl. Phys. A **727**, 233 (2003).